High-Resolution Spectroscopy of CH2D+ in a Cold 22-Pole Ion Trap

ARTICLE *in* THE JOURNAL OF PHYSICAL CHEMISTRY A · APRIL 2013

Impact Factor: 2.69 · DOI: 10.1021/jp400258e · Source: PubMed

6 AUTHORS, INCLUDING:

Sandra Brünken
University of Cologne
88 PUBLICATIONS **1,051** CITATIONS

SEE PROFILE

Stephan Schlemmer
I. Physikalisches Institut, Universität zu Köln
235 PUBLICATIONS **2,899** CITATIONS

SEE PROFILE

THE JOURNAL OF PHYSICAL CHEMISTRY A

Article

pubs.acs.org/JPCA

High-Resolution Spectroscopy of CH_2D^+ in a Cold 22-Pole Ion Trap

Sabrina Gärtner, Jürgen Krieg,[‡] André Klemann,[¶] Oskar Asvany, Sandra Brünken, and Stephan Schlemmer*

I. Physikalisches Institut, Universität zu Köln, Zülpicher Strasse 77, 50937 Köln, Germany

ABSTRACT: The method of laser-induced reaction (LIR) is used to obtain high-resolution IR spectra of CH_2D^+ in collision with n-H_2 at a nominal temperature of 14 K. For this purpose, a home-built optical parametric oscillator (OPO), tunable in the range of 2500−4000 cm^{-1}, has been coupled to a 22-pole ion trap apparatus. In total, 112 lines of the ν_1 and ν_4 bands have been recorded. A line list is inferred from a careful analysis of the shape of the LIR signal. Line positions have been determined to an accuracy of 1×10^{-4} cm^{-1}, allowing for the prediction of pure rotational transitions with MHz accuracy. In addition, an IR-THz double-resonance LIR depletion technique is applied to H_2D^+ to demonstrate the feasibility for pure rotational spectroscopy with LIR.

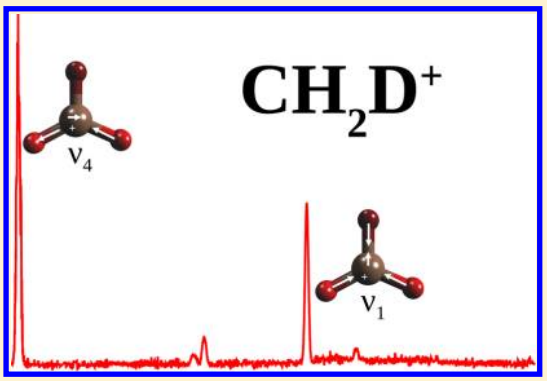

INTRODUCTION

Takeshi Oka pioneered the field of molecular spectroscopy in many ways. In particular, high-resolution infrared spectra of molecular ions have been recorded in his laboratories for a number of key ionic species, among those, the family of carbo-ions (see, for example, Jagod et al.[1] and references therein). CH_2D^+, which is studied in this work, is one of these carbo-ions that was investigated already some 20 years ago. All of these ions play an important role in astrophysics and in various plasma environments. To obtain IR or even FIR spectra of these transient species in the laboratory is a difficult task for a number of reasons. The Oka laboratory was one of those mastering the challenges.

In those experiments, ions were produced in a cooled discharge cell reaching sufficient column densities for IR absorption spectroscopy. Optimizing the discharge conditions for maximum signal of the desired ion helped to disentangle the tremendous number of lines in the C−H stretching region where many carbo-ion spectra overlap. In most cases, the data represented the first high-resolution spectra recorded for these species. They were fitted to standard Watson Hamiltonians and often remain state-of-the-art studies to this day. In many cases, the quality of the model description is high enough to even predict pure rotational spectra of those species. Given the precision and accuracy of the high-resolution data available at that time, rotational lines could be predicted to tens of MHz. As a consequence, these predictions could be used to search for rotational spectra of these molecules in the laboratory and in space.

The narrow line width, high power, stability, and large tuning range of today's continuous-wave (cw) infrared optical parametric oscillators (OPOs) make infrared spectroscopy in the C−H stretching region much more convenient and allow for more sophisticated ion spectroscopy experiments, aiming at the highest resolution. McCall and co-workers, for instance, conduct absorption experiments on molecular ions in a cooled discharge cell employing sophisticated laser schemes to make use of the high resolving power of the OPO systems. A recent example on the sub-Doppler spectroscopy of H_3^+ demonstrates a line center precision below 100 kHz.[2]

In our group, we also seek to obtain infrared spectra at a resolution suitable for predicting rotational spectra with sub-MHz uncertainty. In space observations, it is often the MHz line width of pure rotational transitions at THz frequencies that determines the resolution required to identify a molecule in space. It will be discussed in this work that this level of accuracy should be reached easily with the current techniques. The IR spectroscopy of CH_2D^+ provides an example of low-temperature spectra recorded at high resolution using the method of laser-induced reactions (LIRs), which was developed in our group over the past decade.[3−6] With LIR, in contrast to discharge cells, only a few hundred to thousands of mass-selected ions are stored in the electrical field of a radio frequency ion trap, where they are subject to the laser radiation and to collisions with a reaction gas. Due to mass selection, the confusion of different species can be avoided. The actual line width and the partition function are both reduced by cooling to 14 K in the present case. Due to the low number of trapped ions, absorption spectroscopy is very difficult, if not impossible. Instead, reactions with the neutral collision partner are enhanced by the laser excitation. This enhancement is recorded as an increase of the product signal as a function of the excitation wavelength. This procedure is followed in this work

Special Issue: Oka Festschrift: Celebrating 45 Years of Astrochemistry

Received: January 9, 2013
Revised: April 26, 2013

   dx.doi.org/10.1021/jp400258e | J. Phys. Chem. A XXXX, XXX, XXX−XXX

to record spectra of CH_2D^+ based on reactions of CH_3^+ and its isotopologues in collisions with H_2.

In space, CH_3^+ is quite unreactive in collisions with H_2; therefore, traces of HD lead to the formation of CH_2D^+ and its isotopologues via the exothermic reactions[7,8]

$$CH_3^+ + HD \rightleftharpoons CH_2D^+ + H_2 \quad (1)$$

$$CH_2D^+ + HD \rightleftharpoons CD_2H^+ + H_2 \quad (2)$$

$$CD_2H^+ + HD \rightleftharpoons CD_3^+ + H_2 \quad (3)$$

The first reaction is exothermic by approximately 370 K.[8] This relatively high exothermicity can thus lead to deuterium fractionation in warmer (50 K) molecular clouds, while in colder regions (10 K), similar reactions with lower exothermicities based on H_3^+ isotopologues are dominant. To test this possibility, the firm quantitative detection of the CH_2D^+ isotopologue is a current aim in astrochemistry. A first tentative detection of the $1_{01}-0_{00}$ transition at 278691.8 MHz has been reported[9] toward Orion IRc2, hampered by strong neighboring lines. A further line at 201754.2 MHz ($2_{11}-2_{12}$) is reported in this issue.[10]

The infrared-active rovibrational bands ν_1 and ν_4 of CH_2D^+ at roughly 3005 and 3106 cm^{-1} were first investigated in the Oka group[11,12] with an accuracy of ~0.003 cm^{-1} (90 MHz), leading to the first available predictions of pure rotational lines. Due to the astronomical detection of many deuterated molecules in the last decades, there has been recent interest in CH_2D^+ and a revival of its spectroscopy, with efforts in our group[13] and the first pure rotational lines of CH_2D^+ measured by Amano[14] in a discharge cell.

This paper is a comprehensive account of our earlier work[13] and is organized as follows. First, the 22-pole trapping instrument, the method of LIR, and the narrow bandwidth OPO are described. In the Results and Discussion section, the 112 transitions measured within the bands ν_1 and ν_4 of CH_2D^+ are presented and analyzed. Emphasis is placed on the difference between an absorption signal and the LIR product signal, where the collision with the reaction gas is an intrinsic part of the action spectroscopy. The spectroscopic results lead to line lists, as in conventional spectroscopy, which are further analyzed. Comparison of several combination differences in the ground and excited states confirm the accuracy of the measurements, which are on the order of 10^{-4} cm^{-1}, that is, several MHz. On the basis of the obtained molecular constants, predictions are made for ground-state rotational transitions and compared to the results of Amano.[14] In the concluding section, we describe limitations in the precision and accuracy of line center determination and discuss some improvements to the current experiment, in particular, the application of a frequency comb. Also, the first results for pure rotational spectroscopy using two photons are described.

EXPERIMENTAL ASPECTS

LIRs of CH_2D^+. High-resolution spectroscopy has been performed with the method of LIR.[3−6,15,16] The LIR principle is based on the change in reaction rate of an endothermic reaction due to laser absorption. In this case, the backward direction of reaction 1 is used. This reaction is endothermic by about 370 K. When the frequency of the laser is tuned to a transition of the parent ion CH_2D^+, it gets vibrationally exited by absorbing a photon. Due to this excitation ($E/k \approx 4500$ K), the CH_2D^+ ion may react in a collision with the H_2 molecules present in the trap to form CH_3^+ and HD, as depicted in Figure 1. Therefore, by recording the number of CH_3^+ product ions, an absorption of the parent ion CH_2D^+ can be detected. Without excitation, almost no CH_3^+ signal is detected. Therefore, this method is nearly background-free, mass-selective, and rather sensitive due to the long interaction period, that is, signal integration times (on the order of 500 ms).

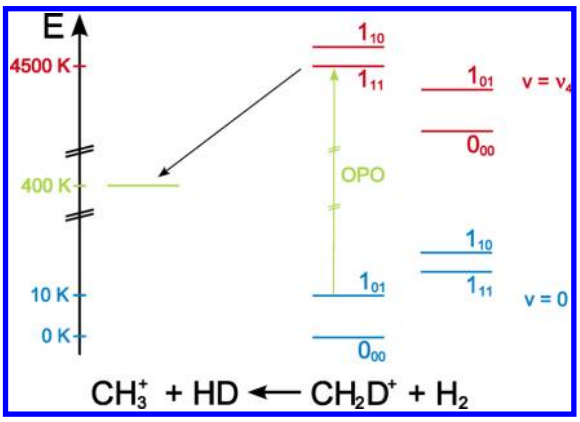

Figure 1. Schematic of the LIR principle. When a CH_2D^+ ion is vibrationally excited by laser radiation, it has enough energy to react with the ambient H_2 to form CH_3^+. In principle, the CH_3^+ ion can then react back to CH_2D^+ with a HD molecule, but this channel can be neglected because there is only the natural amount of $[HD]/[H_2] \approx 3 \times 10^{-4}$ present in the trap.

22-Pole Ion Trap Apparatus. The experiments are conducted with a 22-pole ion trapping apparatus. The ions under investigation are generated by electron impact and trapped by RF fields in a storage ion source. For the production of CH_2D^+, CH_3D gas (Cambridge Isotope Laboratories, Inc.: Methane (D1, 98%)) was used. As helium gas was admitted to the source for cooling the generated CH_2D^+ ions, the ionization energy was kept well below 24 eV to avoid He ionization.

At the beginning of each experimental cycle, a short pulse of ions is extracted from the storage ion source, mass filtered for CH_2D^+ in a quadrupole mass spectrometer, and injected into the 22-pole ion trap.[17] This trap, consisting of 22 RF electrodes forming a cylindrical structure, is mounted on a closed cycle helium refrigerator. Upon entrance, the ions are cooled down to the ambient cryogenic wall temperature (about 14 K) by a short, intense helium pulse. During the storage period of typically 480 ms, the ions are exposed to H_2 gas. For LIR spectroscopy, tunable cw light from an IR OPO (see the next section) is sent through the axially transparent setup. After storage, the ion cloud is extracted into a second quadrupole mass filter, selecting the LIR-generated CH_3^+ ions, which are then counted in a Daly-type detector.[18] This cycle is repeated every 500 ms. By counting the CH_3^+ product ions as a function of the OPO wavelength, a spectrum is recorded.

OPO System. As a radiation source, a home-built cw OPO in the wavelength region around 3 μm has been used. A schematic overview of the OPO setup is depicted in Figure 2. The present setup is analogous to that of an OPO emitting idler radiation of around a 5 μm wavelength, which has been described recently in more detail.[19] It uses effects of nonlinear optics in a lithium niobate crystal (5% MgO-doped periodically poled $LiNbO_3$ (PPLN) from HC photonics, Taiwan) to transfer power from an intense and focused pump laser (Innolight MOPA series, Nd:YAG at 1064 nm wavelength,

dx.doi.org/10.1021/jp400258e | J. Phys. Chem. A XXXX, XXX, XXX−XXX

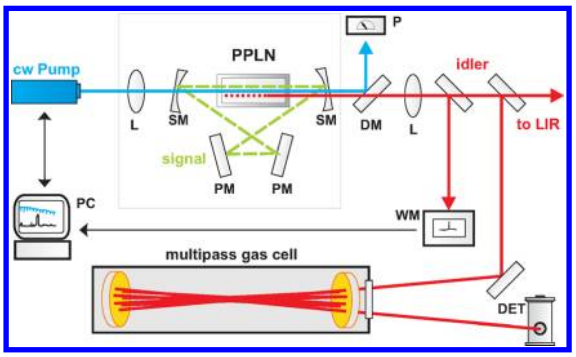

Figure 2. Schematic setup of the OPO system. Abbreviations: L, lens; SM, spherical mirror; PPLN, periodically poled lithium niobate; PM, plane mirror; DM, dichroic mirror; WM, wavemeter; and P, power meter. For details, see the text.

10 W optical power) to two other beams with different wavelengths. These beams are called the signal and idler and are widely tunable. Phase matching of the process is achieved with the seven distinct poling periods of the crystal between 28.5 and 31.5 μm. To enable temperature tuning of the generated waves, the PPLN crystal is held in an oven at temperatures between 50 and 200 °C.

The signal beam that is generated in the OPO process can be tuned between 1.45 and 1.85 μm. It is kept resonant in a high-finesse ring cavity to enhance the conversion process and enable oscillation. The idler beam is the one used for the experiment and can be tuned between 2.5 and 4 μm (2500–4000 cm^{-1}), accordingly. The coating of the mirrors is transparent at idler and pump wavelengths. Optical powers of more than 800 mW are reached in the idler, while the oscillation threshold has been observed at around a 1.5 W pump power. During measurements, the idler power has been selected to be approximately 100 mW by limiting the pump power.

Coarse tuning of the OPO frequency is performed via selection of the crystal poling period ($\Delta\nu/\nu \approx 0.1$ at 3 μm upon changing to neighboring poling period) and crystal temperature in the range of 50–200 °C ($\Delta\nu/\nu \approx 5 \times 10^{-4}$ at 3 μm upon a temperature change of ΔT = 1 K). Continuous tuning of the pump laser (15 GHz mode-hop-free, 80 GHz total) then translates into fine-tuning of the idler beam. At time scales of less than a millisecond, a small line width of better than 1 MHz (3×10^{-5} cm^{-1}) can be estimated for the idler radiation from an experiment with a high-finesse reference cavity with a similar OPO at 5 μm wavelength.[19] This value may also serve as an estimate for the line width of the idler wave used in the present experiments.

For calibration purposes, frequency readouts from a high-resolution wavemeter (Bristol Instruments, model 621-A IR) and transmission through a home-built Herriott-type multipass cell filled with a reference gas (total absorption path length of 50 m) have been recorded simultaneously with the LIR experiment. The use of the absorption cell for absolute calibration is necessary as the wavemeter showed alignment-dependent frequency offsets up to ~0.003 cm^{-1}. For this reason, as mode-hops of the OPO come with a small realignment of the beams, special care has been taken to connect the recorded CH_2D^+ lines to the absolute calibration lines in mode-hop-free scans.

Choice of Calibration Gases. The Herriott-type absorption cell has been filled with calibration gases at low pressure. Due to the high resolution of the system (cold ions combined with a narrow bandwidth laser), only calibration lines with an accuracy better than 4 MHz = 1.3×10^{-4} cm^{-1} could be used for the experiment. In fact, sometimes, the lack of a proper calibration gas absorption line in the (mode-hop-free) tuning vicinity of a measured CH_2D^+ line presented a severe limitation to the current experiment.

Lines of OCS, for example, have been measured with high accuracy using heterodyne techniques (see e.g. Saupe et al.[20]). On the basis of such measurements, calculated line lists can be downloaded from NIST.[21] Due to the mentioned accuracy requirements, only the NIST OCS lines in the range of 3066–3120 cm^{-1} have been used in this work. Additionally, some weaker lines of OCS documented by Guelachvili and Rao[22] have been used, after correcting for an offset value to the more accurate NIST lines. Outside of the mentioned range, water lines in the vicinity of CH_2D^+ lines have been used for calibration. The positions of those lines have been determined by Fourier transform spectroscopy,[23] and again, only the more accurate ones were selected for calibration. For the stronger water absorptions, the amount of H_2O in the laboratory air was sufficient, while for the weaker lines, the Herriott cell was filled with air at low pressure.

RESULTS AND DISCUSSION

Measured Lines. In total, 112 lines in the ν_1 and ν_4 bands have been recorded. A mode-hop-free example scan over 0.4 cm^{-1} is shown in Figure 3. It shows the CH_2D^+ absorption

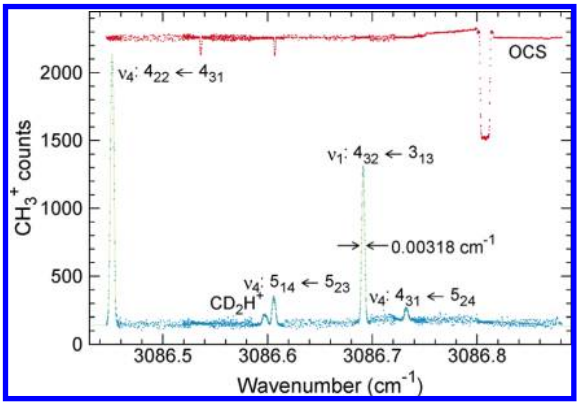

Figure 3. Example of a CH_2D^+ LIR spectrum. For this experiment, the ions were stored in the trap together with the reaction gas H_2 for 480 ms. (Blue) Number of detected CH_3^+ ions; multiple scans were averaged. (Green) Saturated Gaussian line profiles were used to determine the position of the observed lines. (Red) An OCS reference spectrum was recorded simultaniously and is shown here in arbitrary intensity units.

peaks (visible as an increase in the counts of the reaction product CH_3^+) as well as the absorption of the OCS gas in the cell. There are three reference lines in the range of this scan. The positions of the two weaker ones on the left were taken from Guelachvili and Rao[22] by correcting for the offset to the NIST lines. The strong OCS absorption near 3086.8 cm^{-1} is an accurate NIST line, but it is saturated, leading to higher uncertainties in the determination of the calibration line position.

The mass-selective power of the ion trap method allows all measured features to be unambiguously attributed to CH_2D^+, with one of only three exceptions shown in Figure 3. In the

dx.doi.org/10.1021/jp400258e | J. Phys. Chem. A XXXX, XXX, XXX–XXX

process of ionizing the CH_3D gas and storing the produced ions in the source, there are reactions between ions and the neutral gas in the source that lead to a large variety of different ions, including all possible types of $CH_nD_m^+$. Therefore, small impurities of CD_2^+ are coadmitted with CH_2D^+ (both mass 16 au) to the trap and react with the ambient hydrogen immediately to form C D_2H^+ by the reaction

$$CD_2^+ + H_2 \rightarrow CD_2H^+ + H \quad (4)$$

The CD_2H^+ ions can subsequently be excited by the laser and react to form CH_3^+ by

$$CD_2H^+ + H_2 \xrightarrow{h\nu} CH_3^+ + D_2 \quad (5)$$

leading to a LIR signal, as depicted in Figure 3. Because the amount of CD_2H^+ produced in the trap is very small, only its strongest lines are seen. Compared to the CH_2D^+ lines, these appear with small intensities and higher deviation from the Gaussian line profile due to saturation effects, which will be described in more detail in the next section. A further reason for the broader line shape of CD_2H^+ may be the exothermic formation process, eq 4. An enlarged view of the saturated CD_2H^+ peak is provided in Figure 4.

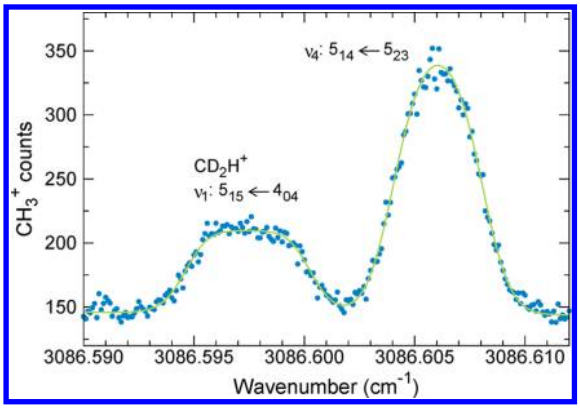

Figure 4. Enlarged view of the CD_2H^+ ν_1:$5_{15} \leftarrow 4_{04}$ and CH_2D^+ ν_4:$5_{14} \leftarrow 5_{23}$ lines. The saturated line profile is given by eq 8, with the parameters $N_0 = 65$, $A{\cdot}t = 4.7$, and $\sigma = 0.00145$ cm^{-1} for the CD_2H^+ line and $N_0 = 250$, $A{\cdot}t = 1.5$, and $\sigma = 0.00138$ cm^{-1} for the CH_2D^+ line.

Tables 1 and 2 provide the measured line positions $\tilde{\nu}_{obs}$. Line positions of CH_2D^+ and of the calibration gases were determined by plotting a model function for a saturated Gaussian line profile (see the next section for details) together with the data and then tuning the parameters such as position, width, intensity, and saturation to get good agreement between the data and the model function. The line position uncertainties were estimated in this process according to the greatest acceptable changes. The uncertainties of the final line positions $\sigma_{\tilde{\nu}}$ given in the tables contain both the uncertainties of the calibration lines and those of the line center determination itself. Also given in the tables are the values obtained by Jagod et al.,[11] $\tilde{\nu}_{jag}$. It is evident that there is a general offset between $\tilde{\nu}_{obs}$ and $\tilde{\nu}_{jag}$, which has to be taken into account when doing a global fit using both data sets.

As already elaborated on in detail by Oka and co-workers,[11] ν_1 and ν_4 are the symmetric a-type stretching and the antisymmetric b-type stretching motions, and the rovibrational transitions thus follow the selection rules $\Delta K_a = 0(\pm 2, \pm 4, \ldots)$, $\Delta K_c = \pm 1(\pm 3, \pm 5, \ldots)$ and $\Delta K_a = \pm 1(\pm 3, \pm 5, \ldots)$, $\Delta K_c = \pm 1(\pm 3, \pm 5, \ldots)$, respectively. The sensitivity of LIR and the high power of the OPO allow transitions with higher-order changes in the quantum numbers K_a and K_c (those given in brackets above) to be detected, as seen in both Tables 1 and 2, extending the already available data set by Oka.[11] For instance, two transitions with $\Delta K_a = -3$, $\Delta K_c = 3$ at 3091.1680, and 3091.6309 cm^{-1} can be found for the band ν_4 in Table 2.

To check the claimed accuracy, combination differences have been calculated. The groups of ground-state combination differences in Table 3 show indeed an excellent agreement within the derived accuracy. Similarly, the 71 measured transitions in the ν_4 band in Table 2 allow for 10 pairs of combination differences in the upper ν_4 vibrational state with also very good agreement. The limited number of measured transitions in ν_1 does not result in any such pairs. Further evaluation of the spectroscopic results is given below. As is evident from the resolved spectral features (e.g., Figure 4), the line profiles can deviate from those of conventional absorption spectroscopy. Because of their relevance for the line center determination, the observed LIR signal line profiles are examined in greater detail in the next section.

Profiles of the LIR Signal. At the beginning of each trapping cycle, a certain number of CH_2D^+ ions is injected into the trap. Once the ions arrive in the trap, they are cooled down to the ambient trap temperature by an intense pulse of helium. Over the full trapping time (480 ms), they are exposed to the radiation field and to collisions with neutral H_2 reaction gas. After absorbing the radiation, they can either react or undergo inelastic collisions with the reactant or the buffer gas. In any moment of the experiment, it is assumed that the ions are thermally equilibrated and therefore show a Maxwell–Boltzmann velocity distribution leading to a Gaussian line profile for absorption

$$g(\tilde{\nu}) \propto e^{-mc^2/2kT[(\tilde{\nu}-\tilde{\nu}_0)/\tilde{\nu}_0]^2} \quad (6)$$

Here, m is the mass of the parent ions, and T is their translational temperature. $\tilde{\nu}$ is the position in the spectrum (in cm^{-1}), $\tilde{\nu}_0$ is the center position of the line, c is the speed of light, and k is the Boltzmann constant. For abbreviation, we use the standard deviation, $\sigma = \tilde{\nu}_0(kT/mc^2)^{1/2}$ (i.e., the Doppler width). The signal strength of the observed lines is influenced by the population of the internal states, which is given by the Boltzmann distribution. We assume the same T for translational and rotational populations.

The spectra taken by LIR spectroscopy develop over the whole trapping time by ions absorbing a photon and then reacting in collisions with H_2. As a result, the number of detected product ions, N_P, increases with the trapping time, t, as

$$N_P(\tilde{\nu}, t) \propto 1 - e^{-K(\tilde{\nu})t} \quad (7)$$

where $K(\tilde{\nu})$ is an effective rate for the laser induced reaction as a net result of excitation, reaction, and other processes. Here, LIR is addressing only a single rotational state of CH_2D^+ in its vibrational ground state, which is thermally populated via a Boltzmann distribution. Thus, only a small number of ions take part in the LIR scheme initially. Due to inelastic collisions, this state is repopulated, leading to the net production of CH_3^+, as stated in eq 7. The early time dependence of LIR has been described for the reaction system N_2^+ + Ar.[3] A more detailed description of LIR kinetics involving quenching mechanisms and other processes has been given for the reaction system $C_2H_2^+ + H_2$.[5,6] In general, the temporal behavior of the product

dx.doi.org/10.1021/jp400258e | J. Phys. Chem. A XXXX, XXX, XXX–XXX

Table 1. Observed Transitions of the ν_1 Band[a] of CH_2D^+

$J'_{K'_aK'_c} \leftarrow J_{K_aK_c}$	$\tilde{\nu}_{obs}$	$\sigma_{\tilde{\nu}} \times 10^5$	$(\tilde{\nu}_{obs} - \tilde{\nu}_{calc}) \times 10^5$	$\tilde{\nu}_{jag}$	$(\tilde{\nu}_{obs} - \tilde{\nu}_{jag}) \times 10^5$
$2_{02} \leftarrow 3_{21}$	2953.70810	12	21		
$4_{40} \leftarrow 5_{41}$	2953.90830	20	12		
$4_{41} \leftarrow 5_{42}$	2954.15290	20	9		
$1_{01} \leftarrow 2_{20}$	2966.49431	20	−2		
$3_{13} \leftarrow 4_{14}$	2972.75642	20	−26	2972.754	242
$2_{20} \leftarrow 3_{21}$	2973.63617	10	10	2973.633	317
$2_{11} \leftarrow 3_{12}$	2973.87663	10	−18	2973.877	−37
$2_{12} \leftarrow 3_{13}$	2980.37367	12	16	2980.372	167
$1_{11} \leftarrow 2_{12}$	2988.23021	40	−74	2988.235	−479
$4_{23} \leftarrow 4_{22}$	2995.37400	12	4		
$0_{00} \leftarrow 1_{01}$	2995.46840	10	−8		
$2_{21} \leftarrow 2_{20}$	3003.32125	40	−21	3003.321	25
$3_{30} \leftarrow 3_{31}$	3003.48600	30	11	3003.485	100
$1_{01} \leftarrow 0_{00}$	3014.01585	20	36		
$2_{02} \leftarrow 1_{01}$	3022.41837	50	3	3022.416	237
$2_{11} \leftarrow 1_{10}$	3025.35013	10	−2	3025.347	313
$4_{13} \leftarrow 4_{14}$	3025.39420	80	176		
$3_{22} \leftarrow 3_{03}$	3026.19814	9	−1		
$3_{03} \leftarrow 2_{02}$	3029.63517	12	−20	3029.635	17
$4_{23} \leftarrow 4_{04}$	3030.39190	50	−45		
$3_{22} \leftarrow 2_{21}$	3031.82203	12	12		
$5_{33} \leftarrow 5_{14}$	3034.21902	30	−31		
$3_{21} \leftarrow 2_{20}$	3034.55695	12	7	3034.556	95
$3_{12} \leftarrow 2_{11}$	3035.02110	10	14	3035.014	710
$4_{14} \leftarrow 3_{13}$	3035.57560	10	4	3035.574	160
$4_{04} \leftarrow 3_{03}$	3036.21680	12	−3	3036.218	−120
$3_{30} \leftarrow 3_{13}$	3048.75405	9	4		
$6_{16} \leftarrow 5_{15}$	3049.19294	20	1	3049.188	494
$6_{06} \leftarrow 5_{05}$	3049.28108	20	−22	3049.28	108
$3_{30} \leftarrow 2_{11}$	3066.11923	15	−14		
$4_{22} \leftarrow 3_{03}$	3071.12714	10	1		
$7_{25} \leftarrow 6_{24}$	3072.00010	20		3071.997	310
$3_{31} \leftarrow 2_{12}$	3072.65881	12	−8		
$4_{31} \leftarrow 3_{12}$	3074.63715	10	3		
$8_{36} \leftarrow 7_{35}$	3075.13560	50	−2	3075.13	560
$5_{32} \leftarrow 4_{13}$	3085.53365	10	6		
$4_{32} \leftarrow 3_{13}$	3086.69140	10	−4		
$5_{23} \leftarrow 4_{04}$	3090.70740	100	−130		
$4_{41} \leftarrow 3_{22}$	3096.42787	8	−1		
$5_{41} \leftarrow 4_{22}$	3099.71230	20	−10		
$5_{33} \leftarrow 4_{14}$	3102.67485	15	5		

[a] $\sigma_{\tilde{\nu}}$ is the experimental uncertainty of the observed line position $\tilde{\nu}_{obs}$. $\tilde{\nu}_{jag}$ are the line positions given by Jagod et al.,[11] with an experimental error of 300×10^{-5} cm^{-1}. The line at 3072.00010 cm^{-1} was not included in the fit because it is very weak and overlaps with a much stronger line. All quantities are given in cm^{-1}.

signal can be more complicated than that given by eq 7; however, the results of this work could be well reproduced by this simple kinetic equation.

In order to illustrate the light-dependent signal of LIR, the temporal evolution for the reaction system $H_3^+ + HD \rightleftharpoons H_2D^+ + H_2$ is displayed in Figure 6. Here, initially stored H_3^+ ions are subject to collisions with H_2 and small quantities of HD in natural abundance in the H_2 gas. The number of H_3^+ ions is decreasing while the number of H_2D^+ ions is increasing due to isotopic exchange. According to the reaction $H_3^+ + HD \rightleftharpoons H_2D^+ + H_2$, an equilibrium ratio of H_3^+ to H_2D^+ is reached after some 1.5 s (see the dashed line extension of the early time dependence in Figure 6). After 0.7 s, laser light from a diode laser is admitted to the trap, exciting the stored H_2D^+ ions to a combination band, as described earlier.[24] The excited H_2D^+ ions are subject to enhanced back reaction to form more H_3^+. As a result, a different H_3^+ to H_2D^+ equilibrium ratio is reached. The temporal behavior of the H_3^+ product ions during the laser interaction is given by the time dependence of eq 7 with a rate $K(\tilde{\nu}) = K(\tilde{\nu}_0)$ at the line center of the rovibrational transition. For the LIR system described in eq 1, the temporal behavior of the product ions is similar. Initially stored CH_2D^+ ions are excited and lead to an enhancement of CH_3^+ product ions. Therefore, the time dependence of the signal follows the late time behavior shown in Figure 6. In order to understand which parameters influence $K(\tilde{\nu})$ in the present case, we will describe the underlying processes in the trap in more detail. See also our earlier work[4,6,15,16] for further information.

The parent ions need to have enough energy to be able to react because we use an endothermic reaction. Upon entrance,

dx.doi.org/10.1021/jp400258e | J. Phys. Chem. A XXXX, XXX, XXX−XXX

Table 2. Observed Transitions of the ν_4 Band[a] of CH_2D^+

$J'_{K'_aK'_c} \leftarrow J_{K_aK_c}$	$\tilde{\nu}_{obs}$	$\sigma_{\tilde{\nu}} \times 10^5$	$(\tilde{\nu}_{obs} - \tilde{\nu}_{calc}) \times 10^5$	$\tilde{\nu}_{jag}$	$(\tilde{\nu}_{obs} - \tilde{\nu}_{jag}) \times 10^5$
$2_{02} \leftarrow 3_{31}$	3034.17340	10	−18		
$3_{31} \leftarrow 4_{40}$	3034.56725	12	−4	3034.565	225
$5_{23} \leftarrow 6_{34}$	3034.65230	20	−10	3034.649	330
$3_{30} \leftarrow 4_{41}$	3034.77728	12	12	3034.775	228
$4_{04} \leftarrow 5_{15}$	3066.14115	10	−2	3066.14	115
$2_{11} \leftarrow 3_{22}$	3066.91140	20	1	3066.911	40
$1_{11} \leftarrow 2_{20}$	3071.09211	10	−8		
$5_{33} \leftarrow 5_{42}$	3072.00010	20	−60	3071.997	310
$4_{32} \leftarrow 4_{41}$	3072.62389	10	0	3072.619	489
$5_{15} \leftarrow 5_{24}$	3072.71760	100	−31	3072.716	160
$3_{03} \leftarrow 4_{14}$	3072.98875	10	−1	3072.988	75
$3_{22} \leftarrow 4_{13}$	3073.68560	10	4	3073.684	160
$1_{10} \leftarrow 2_{21}$	3074.08749	10	2	3074.083	449
$3_{13} \leftarrow 4_{04}$	3074.27680	10	−2	3074.273	380
$5_{05} \leftarrow 5_{14}$	3075.17829	10	−2	3075.176	229
$5_{24} \leftarrow 5_{33}$	3075.96194	10	18	3075.958	394
$4_{14} \leftarrow 4_{23}$	3078.95670	7	−7	3078.951	575
$4_{23} \leftarrow 4_{32}$	3079.24519	7	1	3079.243	219
$2_{02} \leftarrow 3_{13}$	3079.44162	10	−8	3079.438	362
$3_{22} \leftarrow 3_{31}$	3081.22310	10	11	3081.222	110
$2_{12} \leftarrow 3_{03}$	3082.47516	10	−1	3082.473	216
$4_{04} \leftarrow 4_{13}$	3083.63054	10	7	3083.629	154
$3_{31} \leftarrow 4_{22}$	3083.93400	50	−52		
$3_{13} \leftarrow 3_{22}$	3084.16766	15	15	3084.166	166
$3_{21} \leftarrow 3_{30}$	3084.42506	10	−9	3084.424	106
$4_{41} \leftarrow 5_{32}$	3084.53631	51	−16		
$2_{21} \leftarrow 3_{12}$	3085.52922	10	4	3085.526	322
$1_{01} \leftarrow 2_{12}$	3085.83733	10	18	3085.834	333
$6_{24} \leftarrow 6_{33}$	3086.32560	200	45		
$4_{22} \leftarrow 4_{31}$	3086.45169	9	3	3086.449	269
$5_{14} \leftarrow 5_{23}$	3086.60622	10	−2	3086.596	1022
$4_{31} \leftarrow 5_{24}$	3086.73256	10	−1		
$5_{23} \leftarrow 5_{32}$	3087.55431	12	−4	3087.554	31
$2_{12} \leftarrow 2_{21}$	3088.09895	7	2	3088.096	295
$4_{40} \leftarrow 5_{33}$	3088.45050	40	−35		
$4_{04} \leftarrow 3_{31}$	3091.16800	10	10		
$3_{03} \leftarrow 3_{12}$	3091.24687	10	3	3091.245	187
$1_{11} \leftarrow 2_{02}$	3091.49560	10	1		
$5_{05} \leftarrow 4_{32}$	3091.63090	10	−2		
$4_{13} \leftarrow 4_{22}$	3091.68410	10	−16	3091.689	−490
$3_{30} \leftarrow 4_{23}$	3092.48393	12	−11		
$0_{00} \leftarrow 1_{11}$	3092.94730	10	6	3092.944	330
$3_{12} \leftarrow 3_{21}$	3093.96000	10	−1	3093.959	100
$2_{11} \leftarrow 2_{20}$	3094.01180	10	2	3094.013	−120
$2_{02} \leftarrow 2_{11}$	3096.80710	10	−4	3096.805	210
$3_{21} \leftarrow 4_{14}$	3098.33395	20	16		
$2_{20} \leftarrow 3_{13}$	3099.57345	15	1		
$1_{01} \leftarrow 1_{10}$	3099.93800	10	−15	3099.938	0
$5_{15} \leftarrow 4_{22}$	3109.08609	25	3		
$3_{13} \leftarrow 2_{20}$	3111.26786	20	−5		
$1_{10} \leftarrow 1_{01}$	3111.54500	9	18	3111.543	200
$4_{14} \leftarrow 3_{21}$	3112.10835	11	8		
$2_{11} \leftarrow 2_{02}$	3114.41528	11	9	3114.407	828
$3_{21} \leftarrow 3_{12}$	3116.59185	7	−2	3116.59	185
$2_{20} \leftarrow 2_{11}$	3116.93872	9	−15	3116.937	172
$4_{23} \leftarrow 3_{30}$	3117.33931	10	−9		
$4_{22} \leftarrow 4_{13}$	3118.32043	6	3	3118.318	243
$1_{11} \leftarrow 0_{00}$	3118.61329	6	−5	3118.611	229
$3_{12} \leftarrow 3_{03}$	3119.58926	15	−8	3119.589	26
$2_{02} \leftarrow 1_{11}$	3119.88180	15	−13	3119.888	−620

dx.doi.org/10.1021/jp400258e | J. Phys. Chem. A XXXX, XXX, XXX−XXX

Table 2. continued

$J'_{K'_a,K'_c} \leftarrow J_{K_a,K_c}$	$\tilde{\nu}_{obs}$	$\sigma_{\tilde{\nu}} \times 10^5$	$(\tilde{\nu}_{obs} - \tilde{\nu}_{calc}) \times 10^5$	$\tilde{\nu}_{jag}$	$(\tilde{\nu}_{obs} - \tilde{\nu}_{jag}) \times 10^5$
$5_{24} \leftarrow 4_{31}$	3122.54580	10	−9		
$5_{23} \leftarrow 5_{14}$	3122.70310	10	4	3122.701	210
$2_{21} \leftarrow 2_{12}$	3122.90150	10	−1	3122.9	150
$4_{31} \leftarrow 4_{22}$	3123.10070	20	−2	3123.098	270
$3_{12} \leftarrow 2_{21}$	3125.21310	10	2		
$2_{12} \leftarrow 1_{01}$	3125.55645	10	17	3125.556	45
$3_{30} \leftarrow 3_{21}$	3125.63565	10	11		
$3_{22} \leftarrow 3_{13}$	3126.49108	10	−3	3126.492	−92
$4_{13} \leftarrow 4_{04}$	3126.70280	10	15		
$5_{41} \leftarrow 5_{32}$	3132.54970	10	4	3132.553	−330
$5_{33} \leftarrow 5_{24}$	3132.99855	10	1	3132.998	55

[a]The same designations apply as those in Table 1. All quantities are given in cm^{-1}.

Table 3. Comparison of Ground-State Combination Differences $\tilde{\nu}_{cd}$ (in cm^{-1})[a]

band	$J'_{K'_a,K'_c}$	$J^1_{K_a,K_c}$	$J^2_{K_a,K_c}$	$\tilde{\nu}_{cd}$	$\sigma_{cd} \times 10^5$
ν_4	1_{10}	1_{01}	2_{21}	37.45751	13
ν_4	2_{12}	1_{01}	2_{21}	37.45750	12
ν_4	1_{11}	0_{00}	2_{20}	47.52118	12
ν_1	1_{01}	0_{00}	2_{20}	47.52154	28
ν_4	1_{11}	2_{02}	2_{20}	20.40349	14
ν_4	2_{11}	2_{02}	2_{20}	20.40348	15
ν_4	2_{02}	2_{11}	3_{13}	17.36548	14
ν_4	2_{20}	2_{11}	3_{13}	17.36527	17
ν_1	3_{30}	2_{11}	3_{13}	17.36518	17
ν_4	2_{02}	2_{11}	3_{31}	62.63370	14
ν_1	3_{30}	2_{11}	3_{31}	62.63323	34
ν_4	2_{02}	3_{13}	3_{31}	45.26822	14
ν_4	3_{22}	3_{13}	3_{31}	45.26798	14
ν_1	3_{30}	3_{13}	3_{31}	45.26805	31
ν_4	2_{11}	2_{20}	3_{22}	27.10040	22
ν_4	3_{13}	2_{20}	3_{22}	27.10020	25
ν_4	2_{12}	2_{21}	3_{03}	5.62379	12
ν_4	3_{12}	2_{21}	3_{03}	5.62386	19
ν_1	3_{22}	2_{21}	3_{03}	5.62389	15
ν_4	3_{03}	3_{12}	4_{14}	18.25812	14
ν_4	3_{21}	3_{12}	4_{14}	18.25790	21
ν_4	3_{22}	3_{31}	4_{13}	7.53750	14
ν_4	4_{04}	3_{31}	4_{13}	7.53746	14
ν_4	3_{30}	3_{21}	4_{23}	33.15172	16
ν_4	4_{14}	3_{21}	4_{23}	33.15165	13
ν_4	4_{13}	4_{04}	4_{22}	35.01870	14
ν_1	4_{23}	4_{04}	4_{22}	35.01790	51
ν_4	4_{31}	4_{22}	5_{24}	36.36814	22
ν_4	5_{15}	4_{22}	5_{24}	36.36849	103

[a]The uncertainty σ_{cd} considers the uncertainties of the two involved infrared transitions given in Tables 1 and 2. Note that the deviations of combination differences are of the same order as the associated uncertainties.

there will be some parent ions that collide with the reaction gas before they are cooled down by the buffer gas; therefore, there will be an approximately constant background signal of product ions. Therefore, we add a term $+C$ to the number of product ions. After the ions are cooled down, only those ions that have absorbed a photon have enough energy to react. Therefore, we need to take the probability of photon absorption into account. For a single-photon absorption process, this is proportional to

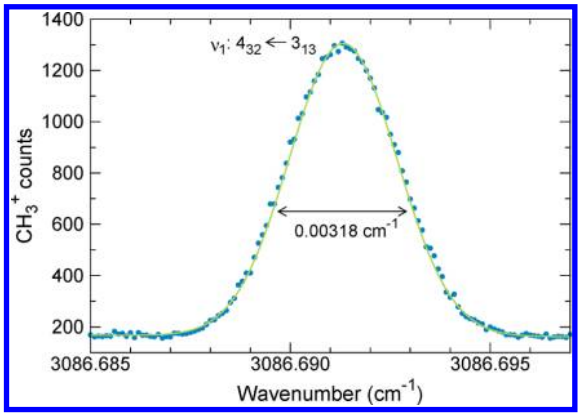

Figure 5. Expanded view of the CH_2D^+ ν_1:$4_{32} \leftarrow 3_{13}$ line, which shows a Gaussian line profile with the number of reacting ions N_0 = 1140 and a fwhm of 0.00318 cm^{-1}, corresponding to an ion temperature of (33 ± 2) K.

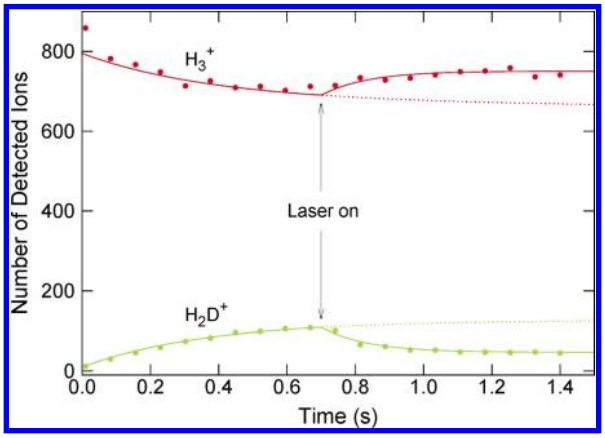

Figure 6. The time evolution of the reaction system $H_3^+ + HD \rightleftharpoons H_2D^+ + H_2$, which is exothermic in the forward direction. In the first 700 ms, no laser radiation is present in the trap; the reaction system evolves toward an equilibrium with high H_2D^+ amount (dotted lines). After 700 ms, infrared radiation, tuned to a strong rovibrational transition of H_2D^+, is applied to the ions. The reaction system evolves toward an equilibrium with a significantly lower amount of H_2D^+. The lines are given by a numerical simulation using the rates $1.9 \times 10^{-9}[HD]$ for the forward reaction, $2.9 \times 10^{-12}[H_2]$ for the backward reaction without the laser, and $1.4 \times 10^{-9}[H_2]$ for the backward reaction with the laser. In the experiment, the nominal trap temperature was about 12 K.

dx.doi.org/10.1021/jp400258e | J. Phys. Chem. A XXXX, XXX, XXX−XXX

the Einstein B coefficient of the observed transition and to the number of photons available and thus to the laser power. The absorption probability depends on the frequency, with the line profile function given in eq 6, due to the Gaussian velocity distribution of the ions. Therefore, we replace $K(\tilde{\nu})$ by $A\ \exp[-(\tilde{\nu} - \tilde{\nu}_0)^2/2\sigma^2]$. Contributions to line broadening due to the laser line width and pressure broadening are negligible under the current experimental conditions. In total, the long time behavior of the number of product ions for the LIR process can be described as

$$N_p(\tilde{\nu}, t) = N_0(1 - e^{-At\cdot e^{-(\tilde{\nu}-\tilde{\nu}_0)^2/2\sigma^2}}) + C(\tilde{\nu}) \quad (8)$$

where N_0 is the number of parent ions available for the reaction.

All experimental lines of this work have been fitted to the profile given by eq 8. No systematic deviations from this behavior have been observed. We take this as justification of the assumptions leading to eq 8. For weak signals, that is, very small values of $A{\cdot}t$, eq 8 can be expanded into a Taylor series

$$N_p(\tilde{\nu}, t) = N_0(At\cdot e^{-(\tilde{\nu}-\tilde{\nu}_0)^2/2\sigma^2} + ...) + C(\tilde{\nu}) \quad (9)$$

leading to a Gaussian LIR profile as observed in most cases; see, for example, Figure 5. For larger values of $A{\cdot}t$, eq 8 yields saturation effects that lead to significant deviations from the Gaussian profile with ever flatter tops of the observed lines, as shown in Figure 4.

The effective reaction rate, and therefore A, increases with the reactivity of the excited ions and with the repopulation rate of the lower state of the transition; any competitive reactions or quenching reduce A. The number of parent ions N_0 that are available for the reaction appears to be the total number of CH_2D^+ ions injected in the trap for most lines; in other reaction systems, we observed substantially lower values for N_0.[5] This might be due to experimental artifacts when some ions are trapped in places not exposed to laser light, even though it is assumed that the ions are thermalized and explore the full volume of the trap, where $E_{kin} + E_{pot} < 3/2kT_{trap}$ holds. In the present experiment, apparently this is not a problem. The possible frequency dependence of the baseline term $C(\tilde{\nu})$ corrects for slight systematic drifts over the long time duration of a frequency scan. The line center frequencies determined from the present line profile analysis have been used for the spectral fitting procedure described in the following.

Fit Results. Spectral fits were done with the standard programs PGOPHER[25] and SPFIT[26] using our data only. Molecular parameters in A reduction for the vibrational ground state and the ν_1 and ν_4 vibrational states have been derived from this analysis and are displayed in Table 4. The fits show consistent results, as long as sextic-order centrifugal distortion constants are included. The corresponding residuals $\tilde{\nu}_{obs} - \tilde{\nu}_{calc}$ are listed in Tables 1 and 2. The weighted residuals $(\tilde{\nu}_{obs} - \tilde{\nu}_{calc})/\sigma_{\tilde{\nu}}$ of the PGOPHER fit are shown in Figure 7 and conform to a normal distribution. The average unweighted deviation of our observed lines to the model is 1.3×10^{-4} cm^{-1}, corresponding to 3.9 MHz. The experimental uncertainties $\sigma_{\tilde{\nu}}$ are only slightly smaller on average. Together with the combination differences given in Table 3, this is taken as evidence of a sound calibration procedure in the LIR studies presented here.

Prediction of Rotational Transitions. On the basis of the model parameters and/or the combination differences, it is possible to predict pure rotational transitions to very high accuracy, as already demonstrated in our previous work.[13] The prediction of pure rotational transitions of CH_2D^+ is significantly improved by the LIR investigations. Table 5 compares the four recently measured pure rotational transitions[14] to the predictions based on the fit given in this work, the fit from the Cologne Database for Molecular Spectroscopy CDMS[27] (based on the data of Rösslein et al.[12] and Jagod et al.[11]), and the current CDMS fit based on all data available. Table 5 demonstrates that the 111 high-resolution IR lines taken into account for the SPFIT[26] fit of this work are already sufficient to make predictions with MHz accuracy suited for astronomical applications, where relative accuracies on the order of 10^{-5} are needed.

Table 4. Best-Fit Molecular Parameters[a] in Ground and Excited Vibrational States of CH_2D^+ Based Only on the Lines Measured in This Work, Given in cm^{-1}

parameter	ground state	ν_4	ν_1
ν		3105.840584(52)	3004.764593(75)
A	9.368512(25)	9.270327(33)	9.210940(47)
B	5.771331(21)	5.732475(15)	5.757158(32)
C	3.525266(21)	3.502936(22)	3.494216(31)
$\Delta_J \times 10^3$	0.12052(31)	0.12249(43)	0.11829(36)
$\Delta_{JK} \times 10^3$	0.3603(17)	0.3450(38)	0.3586(36)
$\Delta_K \times 10^3$	0.2601(24)	0.2988(20)	0.2690(57)
$\delta_J \times 10^3$	0.04772(90)	0.04596(29)	0.0490(12)
$\delta_K \times 10^3$	0.4193(37)	0.3952(48)	0.4105(48)
$\Phi_J \times 10^6$			
$\Phi_{JK} \times 10^6$		0.209(95)	−0.171(89)
$\Phi_{KJ} \times 10^6$	−0.35(12)		0.91(26)
$\Phi_K \times 10^6$			
$\phi_J \times 10^6$	0.024(21)		0.045(20)
$\phi_{JK} \times 10^6$	0.61(13)	−0.26 (18)	0.46 (11)
$\phi_K \times 10^6$			

[a]In total, 35 parameters have been used to fit 111 transitions with SPFIT[26] in A reduction. The numbers in parentheses give the uncertainty of the last digits.

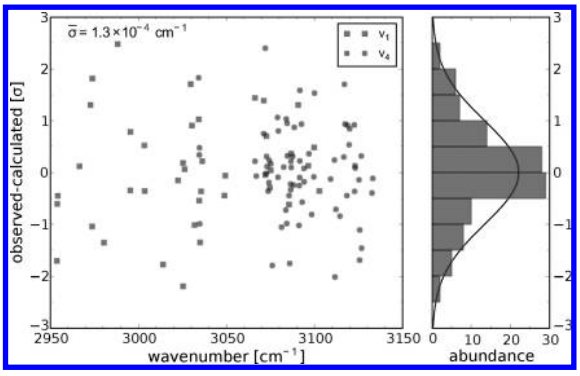

Figure 7. (Left) Residuals of the fit for CH_2D^+ as a function of frequency in units of the individual frequency uncertainty $\sigma_{\tilde{\nu}}$. (Right) Histogram of the residuals. The averaged absolute deviation between the model and observation is $\overline{\tilde{\nu}_{obs} - \tilde{\nu}_{calc}} = 1.3 \times 10^{-4}$ cm^{-1}. The histogram also harbors a plot of the scaled standard normal distribution with $\sigma = 1$ (solid black line).

CONCLUSIONS AND FURTHER EXPERIMENTS

The present experiment demonstrates that the combination of cold ions with a narrow bandwidth laser can yield high-resolution infrared spectra from which pure rotational transitions for the astronomical community can be deduced.

dx.doi.org/10.1021/jp400258e | J. Phys. Chem. A XXXX, XXX, XXX−XXX

Table 5. Comparison of the Four Rotational Transitions of CH_2D^+ Measured by Amano[14] with the Current CDMS[27] Fit (1) Based on the Line Positions of All Available Data[11,12,14] Including This Work, the Previous CDMS Fit (2) Based on the Data from Oka Only,[11,12] and Predictions Based on Our Best-Fit Parameters (3)[a]

$J'_{K'_a,K'_c}$	$J_{Ka,Kc}$	Amano	(1) CDMS	(2) CDMS Oka only	(3) this work
2_{12}	1_{11}	490012.247(30)	−0.012(29)	3.08(416)	−1.18(79)
2_{11}	1_{10}	624492.648(20)	0.000(20)	2.16(570)	−1.59(87)
3_{13}	2_{12}	722354.622(25)	0.011(25)	3.15(592)	1.80(87)
3_{22}	2_{21}	835464.376(50)	−0.016(49)	2.97(620)	0.04(99)

[a]The line positions and the differences prediction − observed are given in MHz. The errors of (1), (2), and (3) are the calculated uncertainties of the prediction.

Applying a cryogenic 22-pole ion trap allowed CH_2D^+ ions to be cooled to a translational temperature of about 30 K (derived from the standard deviation of the Gaussian term), and determining the line center positions of 112 transitions from the ν_1 and ν_4 bands (of which 111 were included in the fit) finally led to predictions of pure rotational transitions with a precision in the range of 1 MHz.

To be able to compete with traditional high-resolution rotational spectroscopy, even higher accuracy and precision is required. One straightforward way to accomplish this is to probe even colder ions, with a lower temperature limit of 4 K when applying buffer gas cooling. Such a 4 K trapping machine is near to completion in our laboratory, and as long as Doppler limited spectroscopy is applied, this will give a modest improvement in precision by a factor of 2 in the near future. An even more important issue is the accurate calibration of the frequency axis. Of the calibration gases used in this work, only the lines of OCS were known with the desired high accuracy and precision, and unfortunately, the lack of adequate calibration gases in some parts of the spectrum forced us to omit some CH_2D^+ lines. Besides this, proper postprocessing calibration is tedious work. Therefore, highly accurate frequency combs, initially developed for atomic spectroscopy and metrology, are increasingly gaining terrain in molecular spectroscopy. Recently, we demonstrated that the combination of our 22-pole ion trap with a commercial OPO and a frequency comb is able to measure rovibrational transitions in the 3 μm range to accuracies well below 1 MHz.[28] Accounting for the improvement of the translational temperature in the near future, we thus aim to measure rovibrational lines with 100 kHz accuracy and precision, thus leading to rotational predictions with errors well below that.

Measuring pure rotational transitions in ion traps is still a challenge, and thus, there are only a few examples.[16,29] The one experiment applying LIR[16] was only feasible due to advantageous molecular parameters of the investigated H_2D^+ ion, namely, its large rotational level spacing (1.37 THz) and its relatively low endothermicity in reaction with H_2. This scheme thus cannot be transferred to other molecular ions in a straightforward manner. For example, pure rotational LIR spectroscopy of CH_2D^+ is nearly impossible due to the low rotational energy gained upon absorption of one photon (higher molecular mass and thus small rotational level spacing) and the high endothermicity of reaction 1 in the backward direction. Therefore, double-resonance experiments are proposed here as a general scheme. In these experiments, infrared and THz radiation are applied simultaneously to the ions. The infrared light is tuned to a vibrational transition starting from one of the levels involved in the pure rotational transition. A THz absorption should then lead to an increase or decrease of the infrared signal, depending on whether the infrared light is tuned on a transition starting from the upper or the lower level of the pure rotational transition, respectively.

A first demonstration of this two-photon rotational scheme is shown in Figure 8. Again, H_2D^+ has been chosen as a test case because it has been explored in our group in great detail previously; therefore, the transitions involved are well-known.[16,24] A commercially available diode laser has been used to excite the H_2D^+ ions into the overtone band (0,2,1) at about 6466 cm^{-1}. The resulting H_3^+ signal has then been disturbed by depleting the starting 0_{00} rotational level by the pure rotational excitation $1_{01} \leftarrow 0_{00}$ at 1.37 THz, leading to a dip in the H_3^+ signal.

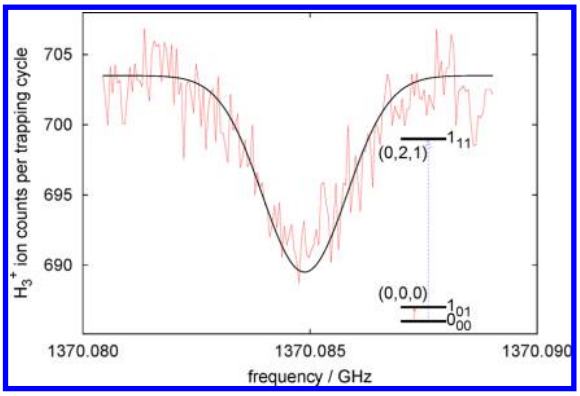

Figure 8. Two-photon rotational spectrum of H_2D^+. The overtone excitation into the (0,2,1) vibrational band[24] (blue dotted line) leads to about 700 H_3^+ signal counts. This signal is then disturbed by depleting the 0_{00} ground-state rotational level by rotational excitation[16] (red solid arrow). The Doppler temperature is about 20 K.

In conclusion, this work shows that spectroscopy at the highest resolution over a very wide frequency range is possible using LIR. Using more advanced Lamb-dip spectroscopy, it may be possible to record spectra with sub-Doppler resolution. The LIR method is extremely sensitive due to the single-ion detection limit and is molecule-specific due to mass selection. It is the method of choice for tackling the most challenging spectroscopic systems like the elusive CH_5^+, a system also pioneered by Oka and co-workers.[30] The combination of trap experiments with the accuracy available in frequency-comb-based spectroscopy can be used to take unbiased spectra in the infrared region, where frequency coverage with an OPO is easily possible. Searching for combination differences might help to unfold the rotational structure of such floppy molecules where searching for pure rotational spectra is very tedious due to the large uncertainties in the molecular constants and hence in the predicted spectra. In the current work on CH_2D^+, we demonstrate these spectroscopic capabilities for a less complicated spectrum.

dx.doi.org/10.1021/jp400258e | J. Phys. Chem. A XXXX, XXX, XXX−XXX

AUTHOR INFORMATION

Corresponding Author

*E-mail: schlemmer@ph1.uni-koeln.de.

Present Addresses

‡J.K.: Miltenyi Biotec GmbH, Bergisch Gladbach, Germany.

¶A.K.: Bosch Rexroth AG, Lohr am Main, Germany.

Notes

The authors declare no competing financial interest.

ACKNOWLEDGMENTS

This work has been financially supported by the Deutsche Forschungsgemeinschaft (DFG) via SFB 956 and SCHL 341/6-1. S. G. and J. K. were supported by the Bonn Cologne Graduate School of Physics and Astronomy (BCGS). We thank Colin Western for his quick help and updates of PGOPHER and Holger Müller for discussions.

REFERENCES

(1) Jagod, M.-F.; Rösslein, M.; Gabrys, M.-F.; Rehfuss, B. D.; Scappini, F.; Crofton, M. W.; Oka, T. Infrared Spectroscopy of Carbo-Ions. VI. C−H Stretching Vibration of the Acetylene Ion $C_2H_2^+$ and Isotopic Species. *J. Chem. Phys.* **1992**, *97*, 7111−7123.

(2) Crabtree, K. N.; Hodges, J. N.; Siller, B. M.; Perry, A. J.; Kelly, J. E.; Jenkins, P. A., II; McCall, B. J. Sub-Doppler Mid-Infrared Spectroscopy of Molecular Ions. *Chem. Phys. Lett.* **2012**, *551*, 1−6.

(3) Schlemmer, S.; Kuhn, T.; Lescop, E.; Gerlich, D. Laser Excited N_2^+ in a 22-Pole Ion Trap: Experimental Studies of Rotational Relaxation Processes. *Int. J. Mass Spectrom.* **1999**, *185*, 589−602.

(4) Schlemmer, S.; Lescop, E.; von Richthofen, J.; Gerlich, D.; Smith, M. A. Laser Induced Reactions in a 22-Pole Trap: $C_2H_2^+ + h\nu_3 + H_2 \rightarrow C_2H_3^+ + H$. *J. Chem. Phys.* **2002**, *117*, 2068−2075.

(5) Schlemmer, S.; Asvany, O. Laser Induced Reactions in a 22-Pole Ion Trap. *J. Phys.: Conf. Ser.* **2005**, *4*, 134−141.

(6) Asvany, O.; Giesen, T.; Redlich, B.; Schlemmer, S. Experimental Determination of the ν_5 Cis-Bending Vibrational Frequency in Ground State ($X\ ^2\Pi_u$) $C_2H_2^+$ Using Laser Induced Reactions. *Phys. Rev. Lett.* **2005**, *94*, 073001.

(7) Asvany, O.; Schlemmer, S.; Gerlich, D. Deuteration of CH_n^+ (n = 3−5) in Collisions with HD Measured in a Low Temperature Ion Trap. *Astrophys. J.* **2004**, *617*, 658−692.

(8) Smith, D.; Adams, N.; Alge, E. Some H/D Exchange Reactions Involved in the Deuteration of Interstellar Molecules. *Astrophys. J.* **1982**, *263*, 123−129.

(9) Lis, D. C.; Goldsmith, P. F.; Bergin, E. A.; Falgarone, E.; Gerin, M.; Roueff, E. Hydrides in Space: Past, Present, and Future In *Submillimeter Astrophysics and Technology: A Symposium Honoring Thomas G. Phillips*; Lis, D. C., Vaillancourt, J. E.; Goldsmith, P. F.; Bell, T. A.; Scoville, N. Z.; Zmuidzinas, J.; ASPCS: San Francisco, CA, 2009; p 417.

(10) Roueff, E.; Gerin, M.; Lis, D. C.; Wootten, A.; Marcelino, N.; Cernicharo, J.; Tercero, B. CH_2D^+, the Search for the Holy GRAIL. *J. Phys. Chem. A* **2013**, DOI: 10.1021/jp400119a.

(11) Jagod, M.-F.; Rösslein, M.; Gabrys, C. M.; Oka, T. Infrared Spectroscopy of Carbo-Ions: The ν_1 and ν_4 Bands of CH_2D^+, and the ν_1 Band of CHD_2^+. *J. Mol. Spectrosc.* **1992**, *153*, 666−679.

(12) Rösslein, M.; Jagod, M. F.; Gabrys, C. M.; Oka, T. Laboratory Infrared Spectra of CH_2D^+ and $HCCD^+$ and Predicted Microwave Transitions. *Astrophys. J.* **1991**, *382*, L51−L53.

(13) Gärtner, S.; Krieg, J.; Klemann, A.; Asvany, O.; Schlemmer, S. Rotational Transitions of CH_2D^+ Determined by High-Resolution IR Spectroscopy. *Astron. Astrophys.* **2010**, *516*, L3.

(14) Amano, T. Submillimetre-Wave Spectrum of CH_2D^+. *Astron. Astrophys.* **2010**, *516*, L4.

(15) Asvany, O.; Padma Kumar, P.; Redlich, B.; Hegemann, I.; Schlemmer, S.; Marx, D. Understanding the Infrared Spectrum of Bare CH_5^+. *Science* **2005**, *309*, 1219−1222.

(16) Asvany, O.; Ricken, O.; Müller, H. S. P.; Wiedner, M. C.; Giesen, T.; Schlemmer, S. High-Resolution Rotational Spectroscopy in a Cold Ion Trap: H_2D^+ and D_2H^+. *Phys. Rev. Lett.* **2008**, *100*, 233004.

(17) Asvany, O.; Bielau, F.; Moratschke, D.; Krause, J.; Schlemmer, S. New Design of a Cryogenic Linear RF Multipole Trap. *Rev. Sci. Instrum.* **2010**, *81*, 076102.

(18) Daly, N. R. Scintillation Type Mass Spectrometer Ion Detector. *Rev. Sci. Instrum.* **1960**, *31*, 264−267.

(19) Krieg, J.; Klemann, A.; Gottbehüt, I.; Thorwirth, S.; Giesen, T.; Schlemmer, S. A Continuous-Wave Optical Parametric Oscillator around 5μm Wavelength for High-Resolution Spectroscopy. *Rev. Sci. Instrum.* **2011**, *82*, 063105.

(20) Saupe, S.; Wappelhorst, M. H.; Meyer, B.; Urban, W.; Maki, A. G. Sub-Doppler Heterodyne Frequency Measurements near 5 μm with a CO-Laser Sideband System: Improved Calibration Tables for Carbonyl Sulfide Transitions. *J. Mol. Spectrosc.* **1996**, *175*, 190−197.

(21) NIST Wavenumbers for Calibration of IR Spectrometers. http://www.nist.gov/pml/data/wavenum/ (2011).

(22) Guelachvili, G.; Rao, K. N. *Handbook of Infrared Standards II*; Academic Press, Inc.: San Diego, CA, 1993.

(23) Toth, R. A. $2\nu_2-\nu_2$ and $2\nu_2$ Bands of $H_2^{16}O$, $H_2^{17}O$ and $H_2^{18}O$: Line Positions and Strengths. *J. Opt. Soc. Am. B* **1993**, *10*, 1526−1544.

(24) Asvany, O.; Hugo, E.; Müller, F.; Kühnemann, F.; Schiller, S.; Tennyson, J.; Schlemmer, S. Overtone Spectroscopy of H_2D^+ and D_2H^+ Using Laser Induced Reactions. *J. Chem. Phys.* **2007**, *127*, 154317.

(25) *PGOPHER*, a Program for Simulating Rotational Structure. C. M. Western: University of Bristol; http://pgopher.chm.bris.ac.uk (2013).

(26) Pickett, H. M. The Fitting and Prediction of Vibration−Rotation Spectra with Spin Interactions. *J. Mol. Spectrosc.* **1991**, *148*, 371−377.

(27) Müller, H. S. P.; Thorwirth, S.; Roth, D. A.; Winnewisser, G. The Cologne Database for Molecular Spectroscopy, CDMS. *Astron. Astrophys.* **2001**, *370*, L49−L52.

(28) Asvany, O.; Krieg, J.; Schlemmer, S. Frequency Comb Assisted Mid-Infrared Spectroscopy of Cold Molecular Ions. *Rev. Sci. Instrum.* **2012**, *83*, 093110.

(29) Shen, J.; Borodin, A.; Hansen, M.; Schiller, S. Observation of a Rotational Transition of Trapped and Sympathetically Cooled Molecular Ions. *Phys. Rev. A* **2012**, *85*, 032519.

(30) White, E. T.; Tang, J.; Oka, T. CH_5^+: The Infrared Spectrum Observed. *Science* **1999**, *284*, 135−137.